IEEE Photonics Journal
An IEEE Photonics Society Publication

Open Access

Highly Sensitive Dual-Core PCF Based Plasmonic Refractive Index Sensor for Low Refractive Index Detection

Volume 11, Number 5, October 2019

Emranul Haque
Subaha Mahmuda
Md. Anwar Hossain, ***Member, IEEE***
Nguyen Hoang Hai, ***Member, IEEE***
Yoshinori Namihira, ***Life Member, IEEE***
Feroz Ahmed, ***Member, IEEE***

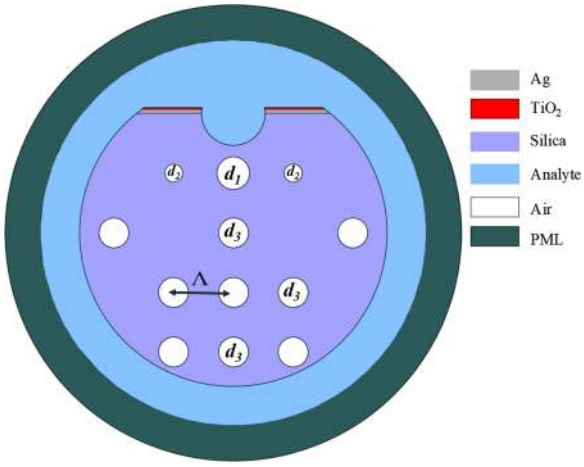

DOI: 10.1109/JPHOT.2019.2931713

IEEE photonics SOCIETY

IEEE

Highly Sensitive Dual-Core PCF Based Plasmonic Refractive Index Sensor for Low Refractive Index Detection

Emranul Haque,[1] **Subaha Mahmuda**,[2] **Md. Anwar Hossain**,[3] ***Member, IEEE***, **Nguyen Hoang Hai**,[4] ***Member, IEEE***, **Yoshinori Namihira**,[5] ***Life Member, IEEE***, **and Feroz Ahmed**,[1] ***Member, IEEE***

[1]Department of Electrical and Electronic Engineering, Independent University, Dhaka 1229, Bangladesh
[2]Department of Electrical and Electronic Engineering, Primeasia University, Dhaka 1213, Bangladesh
[3]Department of Electrical and Electronic Engineering, Green University of Bangladesh, Dhaka 1207, Bangladesh
[4]School of Electronics and Telecommunication, Hanoi University of Science and Technology, Hanoi 100000, Vietnam
[5]University of the Ryukyus, Nishihara 151-0066, Japan

DOI:10.1109/JPHOT.2019.2931713

Manuscript received May 16, 2019; revised June 27, 2019; accepted July 23, 2019. Date of publication July 29, 2019; date of current version August 13, 2019. This work (article processing charge) was supported by Hanoi University of Science and Technology. Corresponding author: Emranul Haque (e-mail: emran1612@iub.edu.bd).

Abstract: A highly sensitive surface plasmon resonance (SPR) sensor on a dual-core photonic crystal fiber (PCF) for low refractive index (RI) detection is presented in this paper. Plasmonic material silver (Ag) is deposited outside of the fiber structure to detect changes of the surrounding medium's refractive index. To prevent oxidation a thin layer of titanium dioxide (TiO_2) is employed on top of the silver. The sensor shows maximum wavelength sensitivity and amplitude sensitivity of 116,000 nm/RIU and 2452 RIU^{-1} with corresponding resolutions (R) of 8.62×10^{-7} and 5.55×10^{-6} RIU, respectively. A thorough study of the relevant literature yielded that these attained sensitivities in both interrogation methods are the highest among reported PCF-SPR sensors to date. In addition, the sensor possesses a very high figure of merit of 2320 in the sensing range of 1.29 to 1.39. Therefore, it would be a suitable candidate for pharmaceutical inspection, organic chemical sensing, and biosensing and other analytes detection.

Index Terms: Surface Plasmon Resonance, Photonic crystal fiber, Refractive index.

1. Introduction

SPR is an optical phenomenon, which happens due to the free electron oscillation on the interface between metallic surface and dielectric layer. In this phenomenon, photons' wavelengths of the incident electromagnetic wave match with the wavelengths of surface electrons under a p-polarized light radiation [1]. Hinge on this process, SPR sensors have been extensively studied due to their attractive characteristics such as electiveness and exactitude in sensing, fast response, real-time and label-free detection, and efficient light-controlling capabilities [2]. The conventional SPR sensors have been designed based on the prism, fiber Bragg grating, slot waveguide and V-groove

waveguide, which make the system bulky and costly [2]. In order to overcome these limitations, SPR sensor based on photonic crystal fiber (PCF) has been proposed which ensures portability, compactness and remote sensing ability. A wide range of PCFs have already been studied with various structures for SPR based sensing applications such as microfluidic slot-based structures, external metal-coated, long-period fiber Bragg grating, and internal metal-coated, and D-shaped structures and so on [2].

PCF based SPR sensor comprises two forms of sensing arrangement: internal and external. In internal sensing, the analyte selectively fills the air holes. This sensing mechanism shows greater sensitivity as implanted analyte directly changes the initial refractive index distribution of the fiber. However, for real-time and distributed sensing application internal sensing method of detection is not feasible. Moreover, this technique is very arduous to execute and also experiences greater propagation loss. These drawbacks of internal sensing can be overcome by placing the analyte on the surface of the PCF, which is known as external sensing technique. Currently, this technique becomes popular due to its simple detection and practical implementation approach [3].

In [4], a gold grating-based PCF-SPR sensor has been introduced with the highest WS of 3340 nm/RIU. A D-shaped PCF sensor accompanied by 1.33–1.43 sensing range with maximum WS of 46000 nm/RIU is reported in [5]. A gold plated D-shaped PCF-SPR sensor is discussed in [6]. The mentioned sensor has a detection range of RI from 1.33–1.38, and the maximum sensitivity of 10,493 nm/RIU which is attained at 1.38. Many other PCF based SPR sensors which are capable of identifying the refractive index of analyte starting from 1.33 are reported in [4]–[14]. Most of these works emphasize on the sensing structures which can only identify analyte having RI greater than 1.33. Very few researches have been conducted on PCF-SPR sensor that can sense the lower RI less than 1.30 [3]. Nowadays there are abundance applications arising where low RI needs to be identified, such as aerogel [15], halogenated ether [16], sevoflurane, pharmaceutical drugs, and so on. Considering this fact some PCF-SPR sensors have been come up in the contemporary time which is apt to sense lower RI of analyte less than 1.30 [16]–[21]. The highest WS of the mentioned sensors are 13500, 6000,11055, 20000,13000 and 51000 nm/RIU, respectively. However, AS has been calculated only in [19], [21] which are about 1054 and 1872 RIU^{-1}, respectively.This indicates enough scope for PCF-SPR sensor able to detect lower refractive index with enhanced sensitivity in both interrogation methods.

In this paper, a dual-core PCF-SPR sensor has been designed and numerically analyzed for low refractive index detection. Double sensing channel created by the microchannel and bimetallic configuration improved the sensing performance in the wavelength as well as amplitude interrogation methods. This is because when TiO_2 is placed on the top of the silver it produces a large number of electrons at the surface which attracts the field from the core to interact firmly with the plasmonic mode. Numerical results indicate maximum spectral and amplitude sensitivities of 116,000 nm/RIU and 2452 RIU^{-1}, respectively. Within the sensing range 1.29–1.39, the obtained lowest resolution of the sensor in the wavelength interrogation method is 8.62×10^{-7}. Effects of parametric variations and possible fabrication technique of the sensor are also explained here thoroughly.

2. Numerical Design and Modeling

The x-y cross-section of the stated sensor is depicted in Fig. 1(a). This proposed sensor architecture is arranged in a square lattice composed of two layers of air hole. Two air holes (d_2) from the top of the first ring have been scaled down to improve the coupling between the core guided and surface plasmon polariton (SPP) modes. To create dual-core another two air holes from the middle of the first ring have been omitted. Fig. 1(b) shows the possible fabrication technique of the proposed sensor. First, all the capillaries and solid rods are stacked together and then draw at a specific rate known as stack and drawn method [5], [9], [19] to fabricate the fiber. Thin, thick capillary and solid rod are used to create big, small and no air holes, respectively [9]. After the fabrication of the fiber is done polishing technique will be applied [5], [13]. By polishing process, part of the fiber plus the large thin wall capillary from the second ring will be polished and the remaining part of the capillary

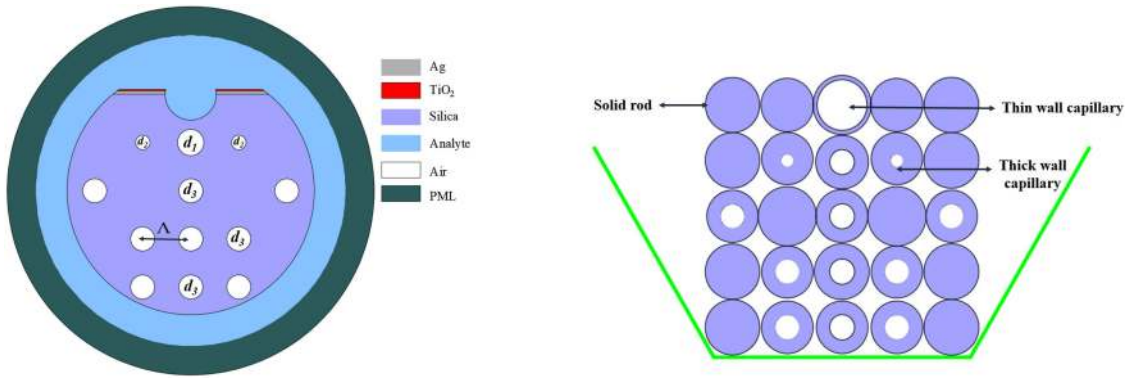

Fig. 1. (a) Schematic diagram of the proposed sensor (b) Stacked preform of the fiber.

produces the microchannel. Chemical deposition method [18], [19], [21] is then applied to coat the silver and TiO_2 on the polished side of the fiber.

The numerical study of the proposed sensor has been done using COMSOL Multiphysics. A perfectly matched layer [22] is added at the outermost layer to absorb radiation power. Physic controlled *extremely fine* mesh element has been used in order to attain maximum simulation accuracy. Optimized parameters of the structure are as follows: $d_1 = 1.80\ \mu$m, $d_2 = 1.00\ \mu$m, $d_3 = 1.65\ \mu$m, pitch $\Lambda = 3.30\ \mu$m, and thickness of the silver and TiO_2 are 65 nm and 10 nm and opening of the microchannel, 1.75 um, respectively. The dielectric constant of the silver is obtained from the Drude model described in [23]. For background material SiO_2 is used whose refractive index is calculated by the following Sellmeier equation as mentioned in [24].

$$n_{si}^2(\lambda) = 1 + \frac{B_1\lambda^2}{\lambda^2 - C_1} + \frac{B_2\lambda^2}{\lambda^2 - C_2} + \frac{B_3\lambda^2}{\lambda^2 - C_3} \tag{1}$$

where, RI of silica is represented by n_{si}, the operating wavelength is denoted by λ in μm and Sellmeier coefficients are specified by B_1, B_2, B_3, C_1, C_2 and C_3.

The dielectric constant of TiO_2 can be defined by the given equation [5].

$$n_{Tio_2}^2 = 5.913 + \frac{2.441 \times 10^7}{\left(\lambda^2 - 0.803 \times 10^7\right)} \tag{2}$$

where, λ is in μm.

3. Result and Discussion

Fig. 2(a,b) depict the field distribution of the core-guided mode and plasmonic mode for the analyte having RI of 1.36. In case of core guided mode, the entire optical field is enclosed in the core. On the other hand, the plasmonic mode is observed on the metal coated sensing medium. The field distribution at the resonance point is presented in Fig. 2(c). Energy transition method between the core-guided fundamental mode and the plasmonic mode as a result of strong coupling effect can also be seen from this figure. In Fig. 2(d), the dispersion affinity of the fundamental mode, plasmonic mode and loss spectra is presented. Refractive indices of the second order SPP mode and the core guided mode intersect each other at the operating wavelength of 1.72 μm for the analytes with RI of 1.36. It is considered here that the excitation of the majority number of free electrons from the surface is responsible for the greater evanescent field in the y-polarized transverse electric (TE) mode TE^y compared to TE^x mode. As the phase matching condition is fulfilled, maximum power transfer can be observed from the core guided fundamental mode to the plasmonic mode. As a result, a peak is observed at the point of intersection.

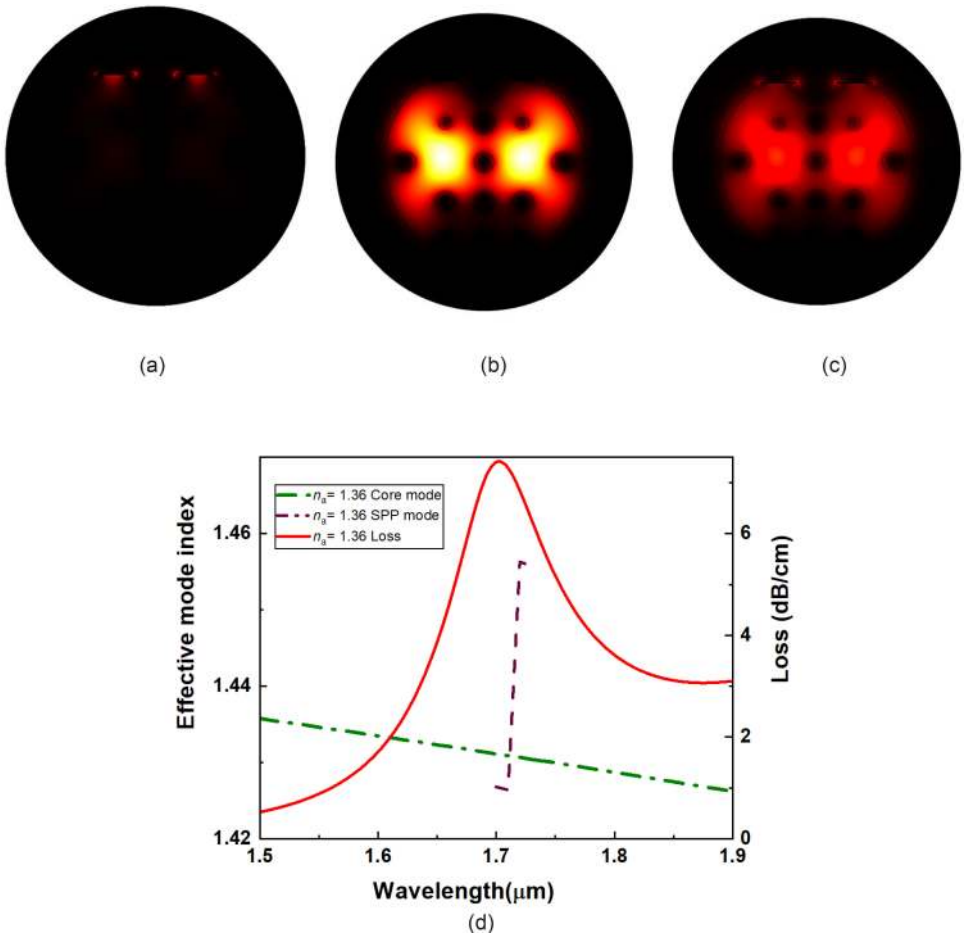

Fig. 2. Optical distribution of n_a 1.36 (a) core mode (b) plasmonic mode (c) resonance condition (d) dispersion relations of core guided mode and SPP mode.

The propagation loss or confinement loss has been calculated by the following equation [5], [21].

$$\alpha = \frac{40\pi \mathrm{Im}\left(n_{eff}\right)}{ln\left(10\right)\lambda} \approx 8.686 \times k_0 \mathrm{Im}(n_{eff}) \times 10^4 \mathrm{db/cm} \tag{3}$$

where, number of waves in free space is specified by, $k_0 = 2\pi/\lambda$, operating wavelength is determined by λ and imaginary part of the effective RI is represented by $\mathrm{Im}(n_{eff})$.

Figure 3(a) presents the loss spectra of the resonant wavelengths while changing the external RI of analyte from 1.29 to 1.39. Due to incomplete coupling, the resonance wavelengths of the sensor experience red shift with increasing propagation loss when the value of RI increases [18]. The R–square value of 0.99 of the polynomial fit indicating a good fitting agreement which is depicted in Fig. 3(b).

WS and resolution can be defined by the equation 4 and 5 [5], [10], respectively. By applying equation 4 and 5, the proposed sensor exhibits maximum WS of 1,16,000 nm/RIU and resolution of 8.62 $\times$ 10^{-7} RIU, respectively. When the analyte's RI changes from 1.29 to 1.39 with a step size of 0.01, the proposed sensor shows wavelength sensitivities of 4000, 4000. 5000, 5000, 6000, 6000, 7000, 9000, 16000 and 116,000 nm/RIU, respectively. The minimum loss is found to be 0.74 dB/cm at the resonance wavelength of 1340 nm while the maximum loss is found to be 829 dB/cm at the resonance wavelength of 3110 nm. Moreover at $n_a = 1.39$, confinement loss is found to be higher due to the strong coupling between core guided and SPP mode. In addition,

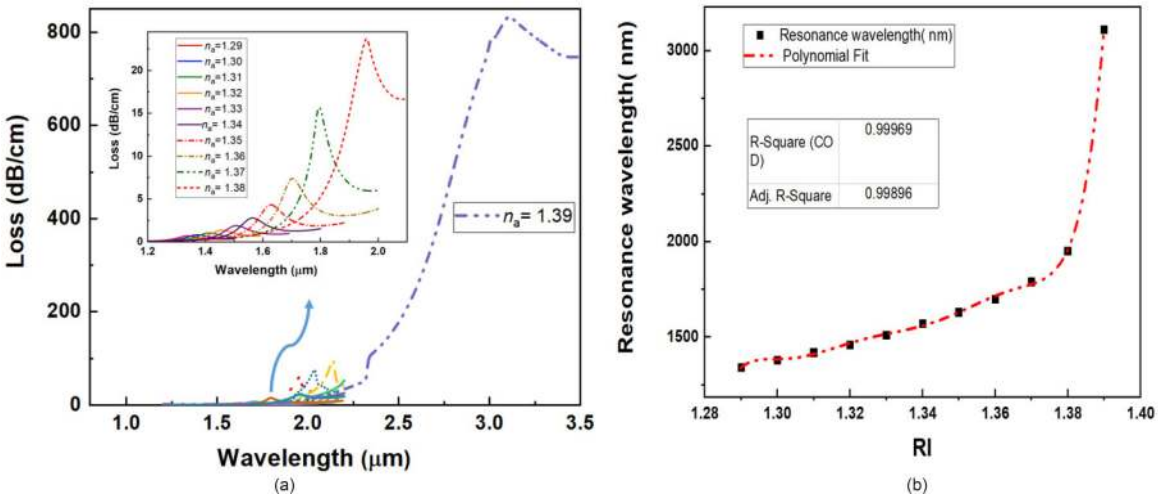

Fig. 3. (a) loss spectra of the sensor for analytes 1.29 to 1.39 (b) Polynomial fit of resonant wavelengths.

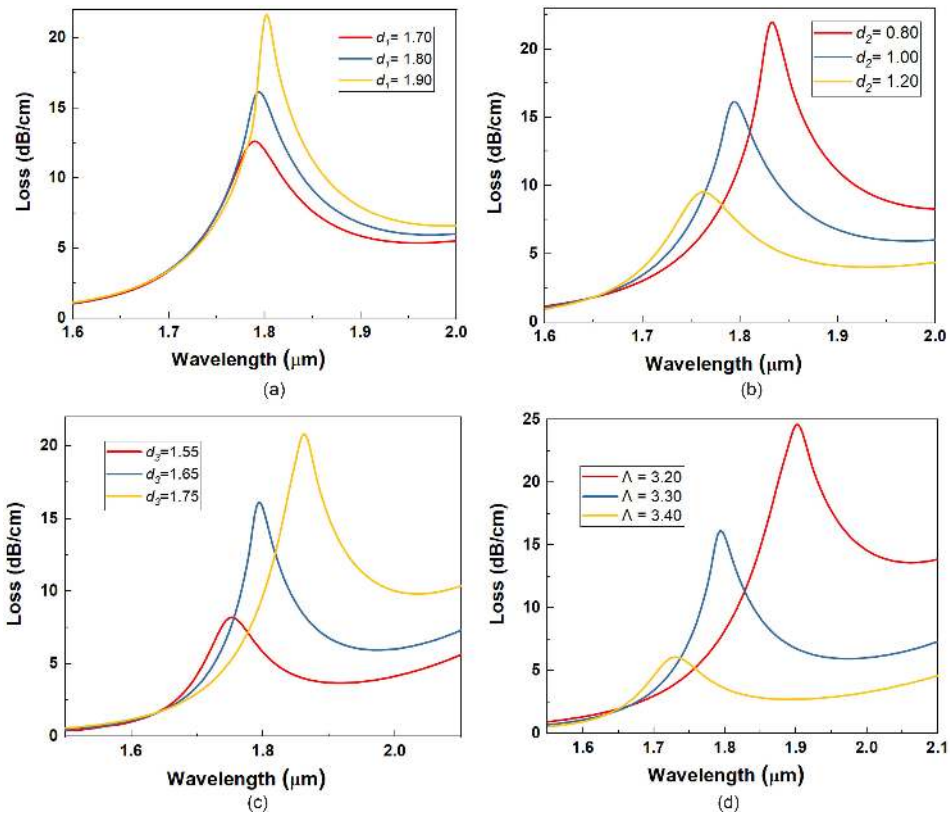

Fig. 4. Loss curve for variation of (a) d_1, (b) d_2, (c) d_3, (d) pitch Λ.

FOM (sensitivity/FWHM) [25] is also calculated and maximum and minimum FOM are obtained 44 and 2320 for the analyte of RI 1.29 and 1.38, respectively.

$$\mathrm{WS[nm/RIU]} = \frac{\Delta\lambda_{peak}}{\Delta n_a} \tag{4}$$

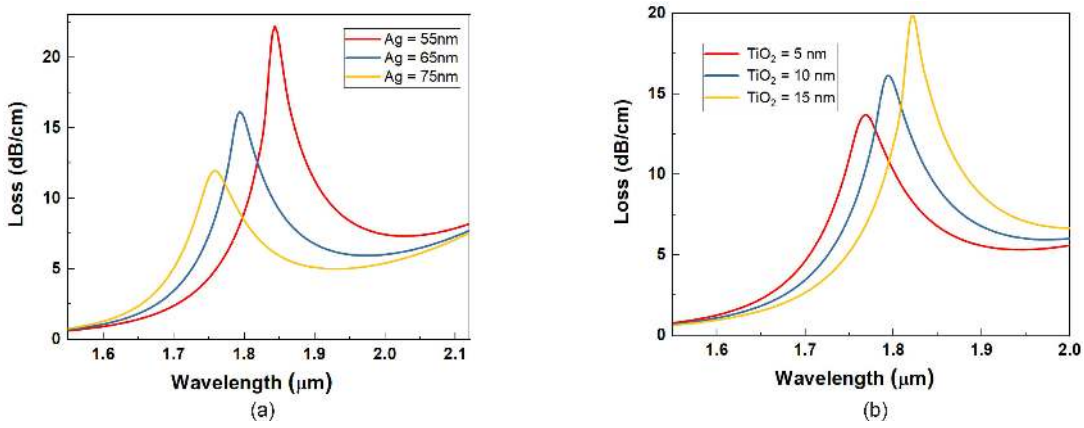

Fig. 5. Loss curves for thickness variation of (a) Ag (b) TiO_2.

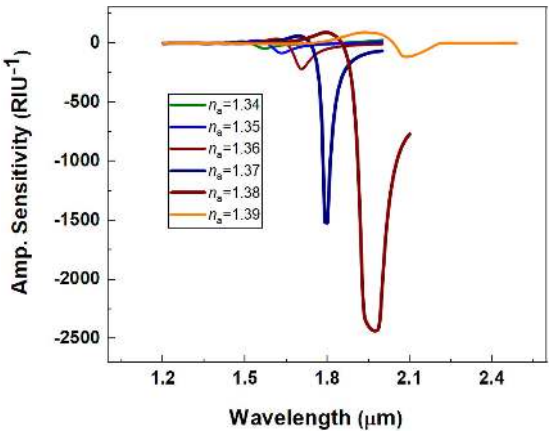

Fig. 6. Amplitude sensitivity with analyte RI changing from 1.34 to 1.39.

where $\Delta\lambda_{peak}$ indicates shift in loss resonance peak and Δn_a specifies change in RI of analyte.

$$R = \Delta n_a \Delta\lambda_{min}/\Delta\lambda_{peak} RIU \tag{5}$$

where $\Delta\lambda_{min}$ represents minimum wavelength resolution and $\Delta\lambda_{peak}$ refers the peak shift of resonance in the wavelength domain.

The impacts of variation of structural parameters (air hole, pitch and metal thickness) on the resonant wavelength of the sensor are investigated for the RI of analyte $n_a = 1.37$ and the results are presented in Fig. 4 and Fig. 5.

When the air hole diameter d_1 increases from 1.70 to 1.90 μm, a red shift is observed in resonant wavelength with high confinement loss as shown in Figure 4(a). Higher confinement loss implies robust coupling within core and SPP mode and vice-versa. As the value of d_2 increases, a blue shift along with reducing confinement loss can be found which is depicted in Fig. 4(b). In Fig. 4(c), a noticeable red shift of resonant wavelength is observed while increasing the value of d_3 from 1.55 to 1.75 μm. For the deviation of pitch $\wedge$ from the value of 3.2 to 3.4 μm, a blue shift followed by low confinement loss is seen in Fig. 4(d).

The influence of silver and TiO_2 thickness on loss spectra are depicted in Figures 5(a) and (b) respectively. When silver layer increases, damping loss also increases. As a result, evanescent field with poor penetration arises, consequence is poor confinement loss [8]. In addition, shifted peak of resonant wavelength can be observed with variation of silver thickness. Because of this fact, as the silver thickness differs from 55 nm to 75 nm, a remarkable blue shift is noticed with decreasing

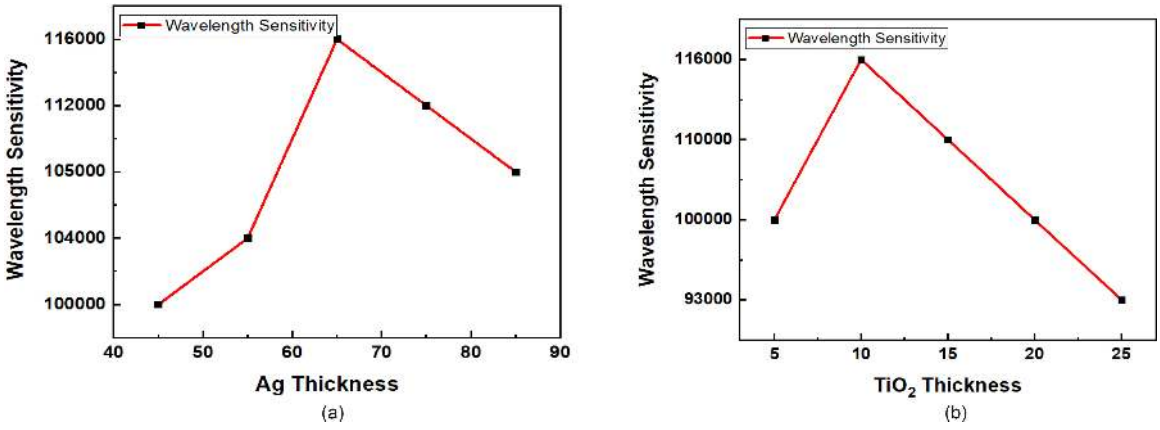

Fig. 7. Wavelength sensitivity for variation of (a) Silver Thickness and (b) TiO_2 Thickness.

TABLE 1
Performance comparison of the proposed sensor with others

Ref.	Max. WS	Max. AS	Lowest. R	Max. FOM	RI Range
[2]	8,000	1560	1.25×10^{-5}	266	1.36-1.41
[5]	46,000	1086	2.2×10^{-6}	--	1.33-1.43
[13]	31,000	--	3.31×10^{-5}	--	1.32-1.40
[14]	62,000	1415	1.6×10^{-6}	1140	1.33-1.43
[16]	13,500	--	7.41×10^{-6}	--	1.27-1.32
[18]	11,055	--	9.05×10^{-6}	--	1.20-1.29
[21]	51,000	1872	1.96×10^{-6}	566	1.22-1.37
[26]	17000	74	5.8×10^{-6}	--	--
[27]	5200	--	1.92×10^{-5}	--	1.33-1.37
proposed	116,000	2452	8.62×10^{-7}	2320	1.29-1.39

propagation loss. When the effective RI of the fundamental mode and SPP mode changes, phase matching condition also changes. As a result, a red shift having rising propagation loss in the resonance wavelength is seen in Fig. 5(b) as the depth of TiO_2 layer increases from 5 nm to 15 nm. Moreover, thicker TiO_2 layer improves the coupling among fundamental mode and SPP mode and the other way around.

AS of the proposed sensor is calculated by using the following AS formula mentioned in [5], the proposed sensor shows the maximum AS of 2452 RIU^{-1} for $n_a = 1.38$ and the minimum of 20 RIU^{-1} for $n_a = 1.29$. Fig. 6(a) depicts AS of the sensor for the variations of analyte RI from 1.34

to 1.39 as an example.

$$A\,S[\mathrm{RIU}^{-1}] = -\frac{1}{\alpha(\lambda, \mathrm{n_a})}\frac{\partial\alpha(\lambda, \mathrm{n_a})}{\partial \mathrm{n_a}} \tag{6}$$

where, the loss for the given analyte with RI n_a is presented by $\alpha(\lambda, n_a)$, the difference between two loss spectra is denoted by $\partial\alpha(\lambda, n_a)$ and change in analyte RI is specified by ∂n_a.

Fig. 7(a) and 7(b) show, how WS differs with different thickness values of silver and TiO_2 respectively. It can be noticed that the highest WS 116000 nm/RIU is attained at 65 nm silver thickness and 10 nm TiO_2 thickness.

The Performances of the proposed sensor are tabulated in Table 1. From Table 1, it is evident that the presented sensor outperformed the recently reported PCF-SPR sensors. Moreover, the record lowest resolution of 8.62×10^{-7} RIU implies that the sensor is able to recognize slight changes of analyte in the 10^{-7} scale which is desirable in the field of bio-sensing [14].

4. Conclusions

A double core highly sensitive plasmonic refractive index sensor for low refractive index detection has been proposed and numerically analyzed. Dual sensing channels induced by microchannel as well as Ag-TiO_2 configuration of the sensor improved the resonance effects significantly resulting in maximum sensitivities of 116,000 nm/RIU and 2452 RIU^{-1} are obtained using wavelength and amplitude interrogation methods, respectively, in the sensing range of 1.29–1.39. Apart from sensitivities, the lowest resolution of 8.62×10^{-7} and maximum FOM of 2320 are also attractive features of the sensor. Moreover, external sensing mechanism and feasible fabrication techniques make the proposed sensor a strong candidate to detect analytes with a lower refractive index like drug monitoring and inspection, bio-organic chemical and so on.

References

[1] Y. Zhan *et al.*, "Surface plasmon resonance-based microfiber sensor with enhanced sensitivity by gold nanowires," *Opt. Mater. Exp.*, vol. 8, pp. 3927–3940, 2018.

[2] M. R. Hasan, S. Akter, K. Ahmed, and D. Abbott, "Plasmonic refractive index sensor employing niobium nanofilm on photonic crystal fiber," *IEEE Photon. Technol. Lett.*, vol. 30, no. 4, pp. 315–318, Feb. 2018.

[3] G. An, S. Li, H. Wang, X. Zhang, and X. Yan, "Quasi-D-shaped optical fiber plasmonic refractive index sensor," *J. Opt.*, vol. 20, no. 3, 2018, Art. no. 035403.

[4] J. Lu, Y. Li, Y. Han, Y. Liu, and J. Gao, "D-shaped photonic crystal fiber plasmonic refractive index sensor based on gold grating," *Appl. Opt.*, vol. 57, pp. 5268–5272, 2018.

[5] A. A. Rifat, R. Ahmed, G. A. Mahdiraji, and F. R. M. Adikan, "Highly sensitive D-shaped photonic crystal fiber-based plasmonic biosensor in visible to near-IR," *IEEE Sens. J.*, vol. 17, no. 9, pp. 2776–2783, May 2017.

[6] G. An, X. Hao, S. Li, X. Yan, and X. Zhang, "D-shaped photonic crystal fiber refractive index sensor based on surface plasmon resonance," *Appl. Opt.*, vol. 56, no. 24, pp. 6988–6992, Aug. 2017.

[7] K. S. Patnaik and R. Jha, "Graphene-based conducting metal oxide coated D-shaped optical fiber SPR sensor," *IEEE Photon. Technol. Lett.*, vol. 27, no. 23, pp. 2437–2440, Dec. 2015.

[8] N. Luan, R. Wang, W. Lv, and J. Yao, "Surface plasmon resonance sensor based on D-shaped microstructured optical fiber with hollow core," *Opt. Exp.*, vol. 23, pp. 8576–8582, 2015.

[9] A. Kumar Paul, A. Krishno Sarkar, A. B. S. Rahman, and A. Khaleque, "Twin core photonic crystal fiber plasmonic refractive index sensor," *IEEE Sens. J.*, vol. 18, no. 14, pp. 5761–5769, Jul. 2018.

[10] M. R. Hasan *et al.*, "Spiral photonic crystal fiber-based dual-polarized surface plasmon resonance biosensor," *IEEE Sens. J.*, vol. 18, no. 1, pp. 133–140, Jan. 2018.

[11] J. N. Dash, R. Das, and R. Jha, "AZO coated microchannel incorporated PCF-based SPR sensor: A numerical analysis," *IEEE Photon. Technol. Lett.*, vol. 30, no. 11, pp. 1032–1035, Jun. 2018.

[12] M. Liu, X. Yang, P. Shum, and H. Yuan, "High-sensitivity birefringent and single-layer coating photonic crystal fiber biosensor based on surface plasmon resonance," *Appl. Opt.*, vol. 57, pp. 1883–1886, 2018.

[13] J. Wu, S. Li, X. Wang, M. Shi, X. Feng, and Y. Liu, "Ultrahigh sensitivity refractive index sensor of a D-shaped PCF based on surface plasmon resonance," *Appl. Opt.*, vol. 57, pp. 4002–4007, 2018.

[14] M. Islam *et al.*, "Dual-polarized highly sensitive plasmonic sensor in the visible to near-IR spectrum," *Opt. Exp.*, vol. 26, pp. 30347–30361, 2018.

[15] T. Bellunato, M. Calvi, C. Matteuzzi, M. Musy, D. L. Perego, and B. Storaci, "Refractive index of silica aerogel: Uniformity and dispersion law," *Nucl. Instrum. Methods Phys. Res.*, vol. 595, pp. 183–186, 2008.

[16] F. Wang, C. Liu, Z. Sun, T. Sun, B. Liu, and P. K. Chu, "A highly sensitive spr sensors based on two parallel PCFs for low refractive index detection," *IEEE Photon. J.*, vol. 10, no. 4, Aug. 2018, Art. no. 7104010.

[17] C. Liu *et al.*, "Birefringent PCF-based SPR sensor for a broad range of low refractive index detection," *IEEE Photon. Technol. Lett.*, vol. 30, no. 16, pp. 1471–1474, Aug. 2018.
[18] X. Chen, L. Xia, and C. Li, "Surface plasmon resonance sensor based on a novel D-Shaped photonic crystal fiber for low refractive index detection," *IEEE Photon. J.*, vol. 10, no. 1, Feb. 2018, Art. no. 6800709.
[19] E. Haque, M. A. Hossain, F. Ahmed, and Y. Namihira, "Surface plasmon resonance sensor based on modified D-shaped photonic crystal fiber for wider range of refractive index detection," *IEEE Sens. J.*, vol. 18, no. 20, pp. 8287–8293, Oct. 2018.
[20] C. Liu *et al.*, "Mid-infrared surface plasmon resonance sensor based on photonic crystal fibers," *Opt. Exp.*, vol. 25, pp. 14227–14237, 2017.
[21] E. Haque, M. Anwar Hossain, Y. Namihira, and F. Ahmed, "Microchannel-based plasmonic refractive index sensor for low refractive index detection," *Appl. Opt.*, vol. 58, pp. 1547–1554, 2019.
[22] M. A. Hossain and Y. Namihira, "Center wavelength adoption techniques for supercontinuum generating highly nonlinear noncircular core photonic crystal fiber," *Japanese J. Appl. Phys.*, vol. 52, no. 5R, 2013, Art. no. 052502.
[23] S. Jiao, S. Gu, H. Yang, H. Fang, and S. Xu, "Highly sensitive dual-core photonic crystal fiber based on a surface plasmon resonance sensor with a silver nano-continuous grating," *Appl. Opt.*, vol. 57, pp. 8350–8358, 2018.
[24] M. A. Hossain *et al.*, "Tailoring supercontinuum generation using highly nonlinear photonic crystal fiber," *Opt. Laser Technol.*, vol. 44, no. 6, pp. 1889–1896, 2012.
[25] A. K. Mishra, S. K. Mishra, and B. D. Gupta, "SPR based fiber optic sensor for refractive index sensing with enhanced detection accuracy and figure of merit in visible region," *Opt. Commun.*, vol. 344. pp. 86–91, 2015.
[26] J. N. Dash, "Highly sensitive side-polished birefringent PCF-based SPR sensor in near IR," *Plasmonic*, vol. 11, no. 6, pp. 1505–1509, 2016.
[27] J. N. Dash and R. Jha, "Highly sensitive D shaped PCF sensor based on SPR for near IR," *Opt. Quantum Electron.*, vol. 48, no. 137, pp. 1–7, 2016.